

Article

Formation and Evolution of Interfacial Structure in Al–Si–Mg/Stainless Steel Bimetals during Hot-Dipping Process

Byung-Joo Kim ¹, Ha-Yoon Lim ¹, Saif Haider Kayani ¹, Yun-Soo Lee ^{1,*}, Su-Hyeon Kim ¹ and Joon-Hyeon Cha ²

¹ Metallic Materials Division, Korean Institute of Material Science, Changwon 51508, Republic of Korea; kbj@kims.re.kr (B.-J.K.); hylim817@kims.re.kr (H.-Y.L.); saifkayani@kims.re.kr (S.H.K.); shawnkim@kims.re.kr (S.-H.K.)

² Steel Supporting Center Task Force Team, Pohang Institute of Metal Industry Advancement, Pohang-si 37666, Republic of Korea; chajh@pomia.or.kr

* Correspondence: yslee@kims.re.kr; Tel.: +82-055-280-3293

Abstract: Understanding trends in the formation of the intermetallic compound (IMC) layer in Al/Fe bimetallic composites can aid in significantly improving their mechanical properties. However, it is currently challenging to predict IMC layer formation during hot-dip aluminizing. Furthermore, the results from previous studies are difficult to compare owing to the variation in the process parameters used. Therefore, to understand how temperatures and holding times affect the thickness and hardness properties of IMC layers, we investigated the interfacial properties of aluminized stainless steel in molten Al–Si–Mg. AISI 420 stainless steel was hot-dip aluminized in an Al–Si–Mg alloy melt for 10–120 min at four different temperatures: 700, 750, 800, and 850 °C. Morphology, type, and element distribution of the phases formed in the reaction layer and the reduction rate of the aluminizing process were studied. Notably, while the reaction layer thickness increased with increasing aluminizing temperature when the holding time was low, long-term reaction caused the reaction layer to become thicker at lower temperatures. The mechanism of this morphological transformation is discussed. The results demonstrated effective trends in controlling the morphology of the intermetallic compound layer with respect to various hot-dip Al plating process parameters.

Keywords: Al–Si–Mg/stainless steel bimetal; hot-dip aluminizing process; phase transformation; hardness properties



Citation: Kim, B.-J.; Lim, H.-Y.; Kayani, S.H.; Lee, Y.-S.; Kim, S.-H.; Cha, J.-H. Formation and Evolution of Interfacial Structure in Al–Si–Mg/Stainless Steel Bimetals during Hot-Dipping Process. *Crystals* **2024**, *14*, 387. <https://doi.org/10.3390/cryst14040387>

Academic Editor: Marek Sroka

Received: 4 April 2024

Revised: 18 April 2024

Accepted: 19 April 2024

Published: 21 April 2024



Copyright: © 2024 by the authors. Licensee MDPI, Basel, Switzerland. This article is an open access article distributed under the terms and conditions of the Creative Commons Attribution (CC BY) license (<https://creativecommons.org/licenses/by/4.0/>).

1. Introduction

Al/Fe bimetallic composites combine the high strength and wear resistance of Fe-based materials such as cast iron and stainless steel (STS) with the heat conductivity, corrosion resistance, and light weight of Al alloys [1], making them highly promising for industrial applications. They have thus attracted significant attention for use in automobile parts such as engine blocks and pistons [2–4].

The liquid–solid composite method is often used to prepare Al/Fe bimetallic composites because of its straightforward process and versatile material choices [5]. Though it is challenging to achieve robust metallurgical bonding owing to the physicochemical differences between Al and Fe [6,7], the removal of the Fe substrate from molten Al results in a pure Al or Al alloy layer adhering to the surface of the intermetallic compound (IMC) layer that forms during the aluminizing process [8]. The adhesion between Al and Fe is influenced by the continuous distribution of this Fe–Al IMC layer [9].

The interfacial bond strength of Al/Fe bimetal is closely related to the thickness of the interlayer. The thickness of the IMC layer is closely related to the interfacial bonding strength of the Al/Fe bimetal. Because of the brittle nature of IMCs, thin reaction layers provide better bonding strength than thicker reaction layers [2,10,11]. Several researchers have therefore attempted to minimize the thicknesses of IMCs in Al/Fe (steel) bimetals by adding alloying elements to the Al melts. Si atoms are particularly pivotal elements. As

the Si content in the Al alloy melt increases, the solid solution of Si in the Fe_2Al_5 phase increases correspondingly [12]. Si atoms then fill the vacancies on the C-axis of the Fe_2Al_5 phase, leading to the formation of ternary Al–Fe–Si IMCs [5]. When Si atoms occupy the vacancies along the C-axis of the Fe_2Al_5 phase, they effectively block the preferred diffusion pathways for Al atoms. This occupation disrupts the facile diffusion of aluminum along the C-axis. These ternary Al–Fe–Si IMCs restrict the diffusion of Al atoms into Fe_2Al_5 , causing a reduction in the Fe_2Al_5 layer thickness. Elements such as Cr and Ni also affect the formation of the reaction layer in STS [5]. However, predicting the formation of the reaction layer in Fe–Cr/Al–Si bimetals remains challenging.

Although numerous studies have been conducted on the development of the aluminizing process, controversy remains regarding phase formation during interfacial reactions in hot-dip aluminizing. The inhibition of the STS/Al reaction by Si is a complex process, and the mechanism underlying the formation of the reaction layer is not fully understood. Furthermore, it is difficult to compare various parameters—such as the composition, reaction temperature, and holding time of the Al alloy and Fe substrate—across studies. Recent studies have often used relatively short hot-dipping times, ranging from 5 to 1800 s [5,12,13]. Considering the potential effects of exposing STS to Al–Si alloys within the aluminizing temperature range of 700–850 °C, it is important to understand how the temperatures and holding time affect the layer thickness and reduction rates. In this study, we investigated the interfacial characteristics of hot-dip aluminized STS in an Al–Si–Mg alloy melt, with a focus on the effects of reaction temperature and holding time on the reaction layer.

2. Materials and Methods

The hot-dip aluminizing process was carried out by immersing the as-received AISI 420 stainless steel rods (hereafter referred to as STS420), which had diameters of 10 mm and lengths of 300 mm (Figure 1a), into a commercial Al–7Si–0.4Mg alloy melt (hereinafter referred to as AC4C). The AC4C alloy, the weight of which was approximately 20 kg (Figure 1a), was melted in an electrical resistance furnace using a crucible with a 30 kg capacity. Table 1 summarizes the chemical compositions of the AC4C and STS420 rods, as determined by optical emission spectrometry (OES; Foundry-Master UV, Oxford Instruments, Abingdon, England). Although the aluminizing process for Al/Fe bimetals is typically performed in the temperature range 700–1100 °C [13,14], excessively high aluminizing temperatures can partially melt the solid material [15]. Hence, the temperature of the molten AC4C alloy was sequentially adjusted to 700, 750, 800, and 850 ± 5 °C for each reaction. Each STS420 rod interacted with the AC4C alloy melt for 10 to 120 min and was then extracted, as illustrated in Figure 1b. Figure 1c exhibits the morphologies of the AC4C/STS420 bimetal samples aluminized at various holding times and reaction temperatures. Under all the aluminizing conditions, the AC4C alloy adequately coated the STS420 rods. An X-ray diffraction (XRD) measurement was used to identify the phases of the STS420 rod and Al–Si–Mg/STS420 bimetals. Data were collected using an XRD instrument (Rigaku International Corp., D/Max 2500VL/PC, Tokyo, Japan) with Cu $K\alpha$ radiation from 20 to 80 (2θ) at a scan rate of $2^\circ/\text{min}$. Figure 1a shows the XRD result and BSE image of the STS420 rod. In the XRD pattern of the STS 420 rod, peaks corresponding to the (111), (200), and (211) planes are clearly observed, and no oxide layer is observed at the interface region (BSE image in Figure 1a).

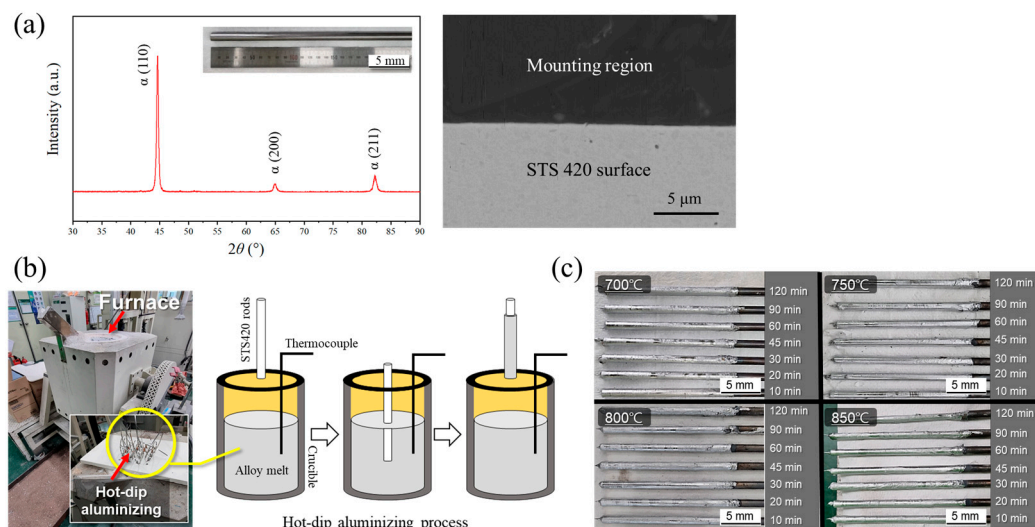


Figure 1. (a) XRD pattern and BSE images of STS 420 rod; (b) hot-dip aluminizing equipment and process schematic; (c) photographs of AC4C/STS420 bimetal specimens aluminized under various process conditions.

Table 1. Chemical compositions of AC4C and STS 420 materials.

Alloy	Composition (wt. %)										
	Al	Fe	Cr	Si	Mg	Mn	Zn	P	Ti	Pb	C
AC4C	Bal.	0.151	-	7.630	0.410	<0.003	0.019	-	0.046	0.013	<0.003
STS420	<0.003	Bal.	13.53	0.451	-	0.543	<0.003	0.024	<0.003	<0.003	0.341

The metallographic specimens were taken from a cross-section 30 mm from the bottom of AC4C/STS420 bimetal and mechanically polished using standard procedures up to colloidal silica for 20 min. The interfacial structure in the AC4C/STS420 bimetal was characterized by an optical microscope (OM; Nikon Eclipse MA200, Tokyo, Japan), field-emission backscattered electron/energy-dispersive spectroscopy (FE-SEM/EDS; JSM-7001F, JEOL Ltd., Tokyo, Japan), and atomic distribution and line scans of the interface region were measured using electron probe microanalysis (EPMA; JXA-8530F, JEOL Ltd., Tokyo, Japan). The thicknesses of the interfacial layer were performed using IMT Isolution DT (ver. 26.5, British Columbia, Canada). Micro-Vickers hardness testing was performed on the interface region of AC4C/STS420 bimetal using a Mitutoyo HM-102 hardness tester (Mitutoyo, Kanagawa, Japan), with a load of 10 g (HV0.1) and a dwell time of 15 s.

3. Results and Discussion

Figure 2 shows the XRD pattern of the AC4C/STS420 bimetals reacted at 700–850 °C for 30 min. For all four bimetals, peaks corresponding to the Fe, Al, Fe₂Al₅ and Al₈Fe₂Si, and FeAl₃ phases were identified. Phase identification at the interface of AC4C/STS420 bimetals was further investigated using EPMA. Figure 3 shows the Fe, Cr, Al, and Si distributions on the interface regions of AC4C/STS420 bimetal aluminized at 700 °C and 850 °C for 60 min, as determined by EPMA. Figure 3c,d exhibit the EPMA line scanning analyses corresponding to the IMC layer identified in Figure 3a and b, respectively. The results confirmed that the Fe and Cr contents in the IMCs increased with increasing proximity to the STS420 surface. The IMC layers stacked on the STS420 surface comprised Fe₂Al₅ and Al₈Fe₂Si phases with about 5 wt.% Cr. The Fe₂Al₅ layer formed parallel to the STS420 surface and exhibited uniform layer thickness. The Al₈Fe₂Si layer, which formed after the Fe₂Al₅ layer, exhibited different morphologies depending on the aluminized temperature. The cross-sectional BSE micrographs of the reaction layers are given in Figure 4. At a reaction temperature of 700 and 750 °C, a flat and linear Al₈Fe₂Si layer was observed

between Fe_2Al_5 and AC4C (Figure 4a,b). When increasing the reaction temperature to 800 and 850 °C, block-shaped $\text{Al}_8\text{Fe}_2\text{Si}$ structures formed on the Fe_2Al_5 layer (Figure 4c,d). This formation of block-shaped $\text{Al}_8\text{Fe}_2\text{Si}$ phases has also been reported in previous aluminizing studies [12,16]. These microstructures suggest that the $\text{Al}_8\text{Fe}_2\text{Si}$ phase grew from the Fe_2Al_5 phase during solidification. The phase compositions, microstructures, and growth sequences of the IMCs formed at the interface were similar to the results obtained in previous studies of Al-Si/(Fe or steel) bimetal [4,7]. Wang et al. also confirmed that the IMC layer of Al-10Si/Fe bimetal aluminized at 700 °C for up to 30 min contains Fe_2Al_5 , $\text{Al}_8\text{Fe}_2\text{Si}$, and $\text{Al}_8\text{Fe}_2\text{Si}_2$ [12]. During the aluminizing process in Al-Si melt, the $\text{Al}_{13}\text{Fe}_4$ phase that forms after the Fe_2Al_5 phase transitions to $\text{Al}_8\text{Fe}_2\text{Si}$ with increasing Si content. The Si content of AC4C (in this study) is approximately 7.6 wt.%, which may explain why other types of Al-Fe compounds are not observed. Additionally, the plate-like $\text{Al}_9\text{Fe}_2\text{Si}_2$ phase commonly reported in Al-Si/Fe bimetal [5,12] was not observed in this study, which may be due to Cr diffusing from STS 420 into the AC4C melt. Elements such as Cr [17], Mn [18], and Co [19] have been reported to induce the transformation of the plate-like Al-Fe-Si phase into the Al(Fe,Cr)Si phase, resulting in the absence of the $\text{Al}_9\text{Fe}_2\text{Si}_2$ phase in several cast Al-Si-Fe-Cr alloys [20]. The $\text{Al}_8\text{Fe}_2\text{Si}$ phase reacts with the liquid to form $\text{Al}_9\text{Fe}_2\text{Si}_2$ by a peritectic reaction at 640 °C: $\text{Al}_8\text{Fe}_2\text{Si} + \text{liquid} \rightarrow \text{Al}_9\text{Fe}_2\text{Si}_2 + \text{Al}$ [12]. The diffused Cr likely prevented the formation of $\text{Al}_9\text{Fe}_2\text{Si}_2$, which could solidify during the cooling process after hot-dip aluminizing.

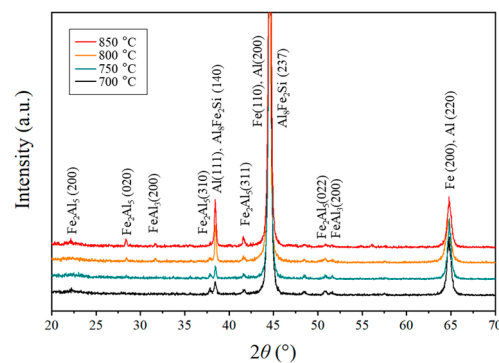


Figure 2. XRD pattern of AC4C/STS 420 bimetal aluminized at different temperatures for 30 min.

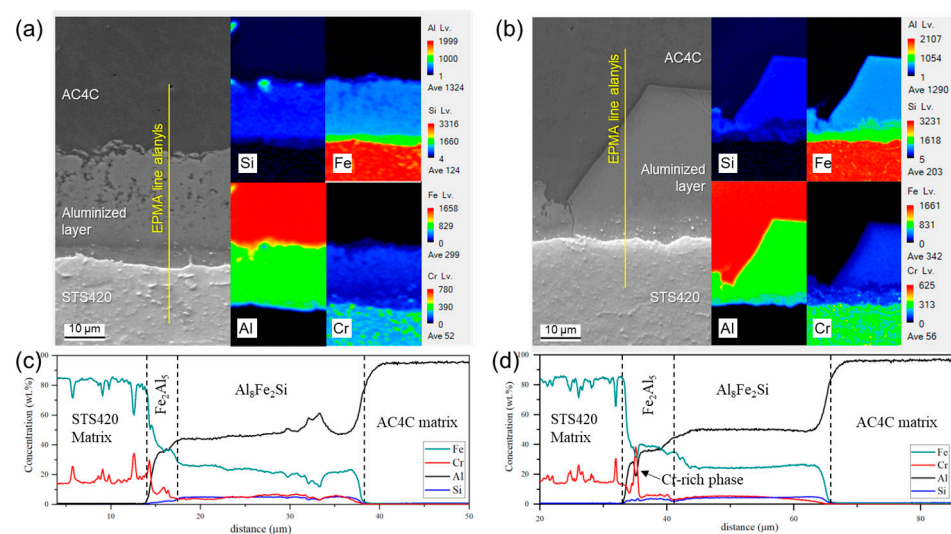


Figure 3. BSE/EPMA mapping and line scanning analysis of the interface region in AC4C/STS420 bimetal aluminized at 700 °C (a,c) and 850 °C (b,d) for 60 min.

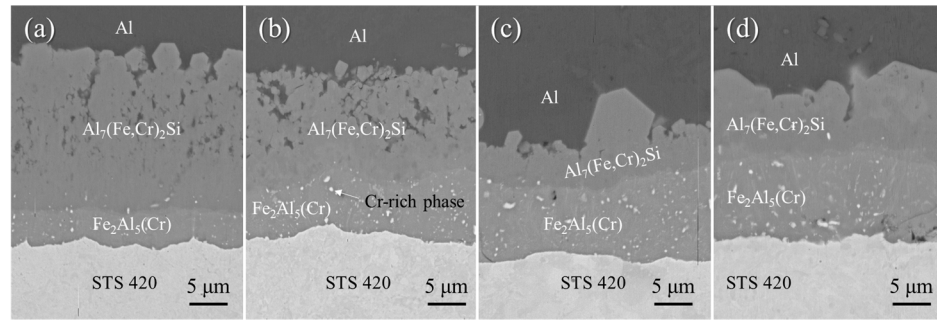


Figure 4. BSE images of the interfacial region of AC4C/STS 420 bimetals reacted at different temperatures for 30 min: 700 °C (a), 750 °C (b), 800 °C (c), and 850 °C (d).

Figure 5 shows high-magnification images of the interfacial region in AC4C/STS420 after reacting at 800 °C for 120 min. The results of the EDS analysis of points 1–7 in Figure 5 are listed in Table 2. This helped further identify each phase in the IMC layer, which was layered with the Fe_2Al_5 and $\text{Al}_8\text{Fe}_2\text{Si}$ phases. The aluminized layer next to the STS420 substrate was broad and primarily comprised the Fe_2Al_5 phase, within which fine Cr-rich precipitates (point 3, indicated in Figure 5a) were uniformly distributed. Cr can dissolve up to 6 wt.% in the Fe_2Al_5 phase, and excess Cr can precipitate out of this phase. Since the Cr content of STS 420 is about 13.4 wt.%, the white particles present in the Fe_2Al_5 phase in Figure 4 are assumed to be precipitated by excess Cr. The Fe_2Al_5 phase containing similar Cr particles was also previously reported in aluminized STS 430 [16]. In the Al-Cr-Fe ternary system [21], Al_8Cr_5 may coexist with the Fe_2Al_5 phase among the Cr-rich precipitates.

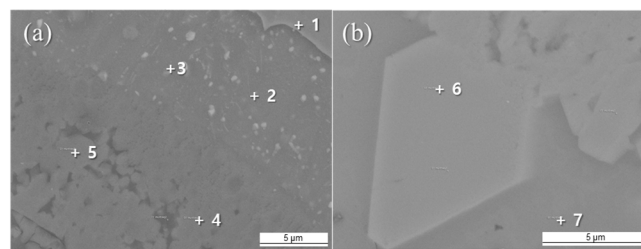


Figure 5. BSE images of different locations in the interface region in AC4C/STS420 bimetal fabricated at 800 °C for 120 min; (a) adjacent to the STS420 substrate and (b) adjacent to the Al top coat.

Table 2. EDS analysis results of the IMC layers in AC4C/STS420 bimetals (points 1–7 in Figure 5).

Point	Composition					Corresponding Phase
	Al (at.%)	Si (at.%)	Cr (at.%)	Fe (at.%)	Mn (at.%)	
1	-	0.73	11.90	87.37	0.82	Fe
2	63.64	5.96	4.30	26.10	0.20	$\text{Fe}_2\text{Al}_5(\text{Cr})$
3	48.57	3.51	23.96	23.96	0.48	Cr rich phase
4	69.21	11.60	3.59	15.60	-	$\text{Al}_8(\text{Fe,Cr})_2\text{Si}$
5	70.98	10.55	3.84	14.63	-	$\text{Al}_8(\text{Fe,Cr})_2\text{Si}$
6	72.05	9.14	3.41	15.40	-	$\text{Al}_8(\text{Fe,Cr})_2\text{Si}$
7	98.96	1.04	-	-	-	Al

Figure 6a shows the OM images of the interface regions of AC4C/STS420 bimetals prepared at 700, 750, 800, and 850 °C under various aluminizing times. Increasing the temperature and aluminizing time resulted in a clear systematic change in the surface morphology. At reaction temperatures of 700 and 750 °C, distinct Fe_2Al_5 and $\text{Al}_8\text{Fe}_2\text{Si}$

layers with comparable thicknesses were observed to be aligned with the STS420 surface. When hot-dipping aluminized at 700 °C for 10 min, the average thicknesses of the Fe_2Al_5 and $\text{Al}_8\text{Fe}_2\text{Si}$ layers were 3.1 and 11.8 μm , respectively. These thicknesses increased with holding time; extending the duration to 120 min caused the average thicknesses of the Fe_2Al_5 and $\text{Al}_8\text{Fe}_2\text{Si}$ layers to increase to 19.5 and 22.2 μm , respectively. These results agree with those in a study by Wang et al., who reported that in Al–Si/Fe bimetals aluminized at 700 °C, the IMCs Fe_2Al_5 and $\text{Al}_8\text{Fe}_2\text{Si}$ form sequentially, and that the thickness of the reaction layer increases with increasing reaction time [12]. Meanwhile, when the reaction temperature was increased from 700 to 750 °C and maintained for 120 min, the trend changed: the thickness of the Fe_2Al_5 layer increased from 19.5 to 23.0 μm , but that of the $\text{Al}_8\text{Fe}_2\text{Si}$ layer reduced from 22.2 to 13.2 μm . When the reaction temperature was further increased to 800 and 850 °C, the Fe_2Al_5 layer changed into a wavy structure and its thickness remained relatively similar (approximately 7–10 μm), even when the reaction time was increased. Though a small amount of block-shaped $\text{Al}_8\text{Fe}_2\text{Si}$ phase was observed even at a reaction temperature of 750 °C when a flat reaction layer formed, the block-shaped $\text{Al}_8\text{Fe}_2\text{Si}$ phase became relatively coarser and more irregular when formed at reaction temperatures of 800 and 850 °C, making it challenging to measure the average thickness of the layer. While the formation of block-shaped $\text{Al}_8\text{Fe}_2\text{Si}$ phases at 650 [16] and 700 °C [12] has been reported in previous aluminizing studies, in the present study, the block-shaped IMC began to form at 750 °C, with major growth occurring at temperatures exceeding 800 °C.

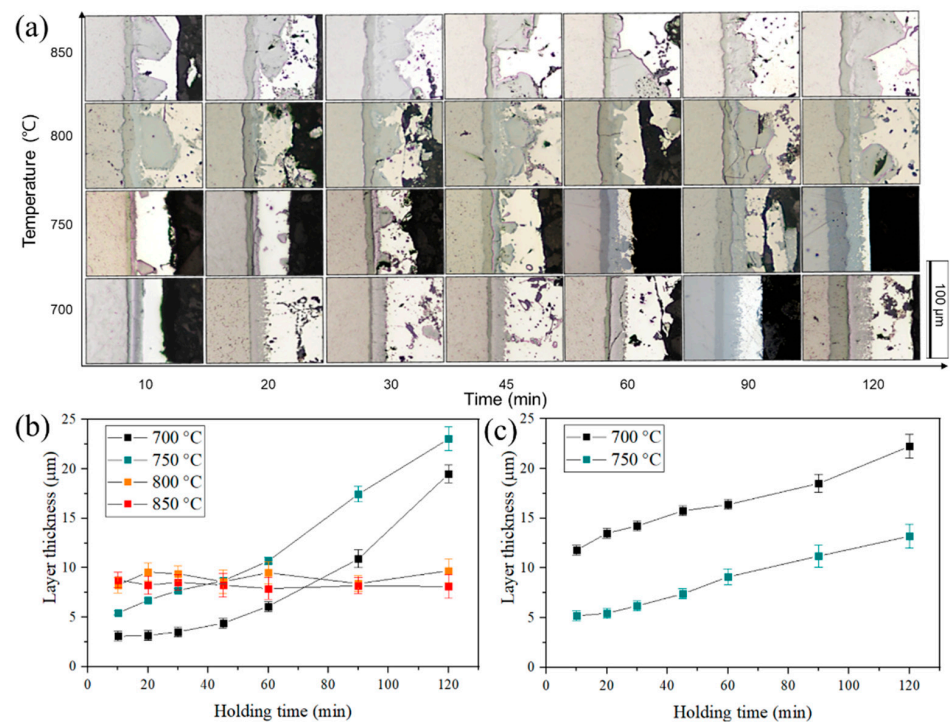


Figure 6. (a) OM images of the interfaces of AC4C/STS420 bimetal specimens fabricated at various aluminizing conditions and change in thickness of the IMC layers as influenced by reaction temperature and holding time: (b) Fe_2Al_5 and (c) $\text{Al}_8\text{Fe}_2\text{Si}$.

Figure 7 shows a schematic of the interfacial reaction of the AC4C/STS420 bimetal. During hot-dip aluminizing, a solute gradient region is created in the Al alloy melt by Fe and Cr atoms diffusing from the STS surface (Figure 7a). At a reaction temperature of 700 °C, the Fe_2Al_5 reaction layer grew uniformly as Al and Si atoms diffused into the STS substrate (Figure 3a). Previous studies have reported that the addition of Si to a molten Al alloy hinders the growth of Fe_2Al_5 , resulting in a flat reaction layer [10,12]; the uniformity of the flat Fe_2Al_5 layer is influenced by the Si concentration in the molten Al alloy [10].

Chemical composition analysis showed that the STS and Fe_2Al_5 substrates contained Si concentrations of approximately 0.73 and 3.51 wt.%, respectively (Figure 5 and Table 2), indicating that the Si atoms in the AC4C melt diffused easily into the STS substrate. As the aluminizing temperature increases, the IMC layer is expected to transform more rapidly due to the higher diffusivity of atoms at elevated temperatures [11]. When the reaction temperature was 850 °C, the Fe_2Al_5 layer grew in an unstable wavy shape owing to the relatively high diffusivity of Fe and Al atoms (Figure 7c). During the cooling process after aluminizing, the diffusion of alloying elements in the remaining molten metal provides the necessary driving force for the formation of intermetallic phases [12].

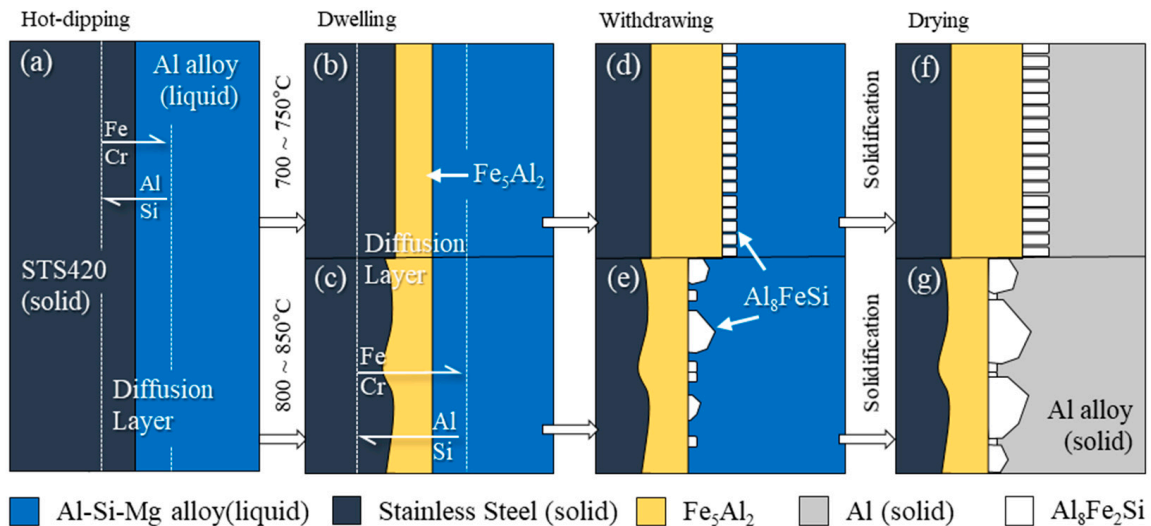


Figure 7. Schematics of phase formation sequence in AC4C/STS420 interface during aluminizing process. (a) Diffusion dissolution layer forms during the initial stages of the aluminizing process. The Fe_2Al_5 layer forms during the reaction step: reaction temperatures of (b) 700 °C and (c) 850 °C. The $\text{Al}_8\text{Fe}_2\text{Si}$ phase nucleates and grows on the Fe_2Al_5 layer until solidification is complete: reaction temperatures of (d,f) 700 °C and (e,g) 850 °C.

The morphology of the $\text{Al}_8\text{Fe}_2\text{Si}$ phase changed from flat (Figure 7d) to block-shaped (Figure 7e) as the melting temperature increased. The $\text{Al}_8\text{Fe}_2\text{Si}$ phase formed after the Fe_2Al_5 layer (Figures 3 and 4) and appeared to grow in the Fe-rich region of the Al melt during solidification. The $\text{Al}_8\text{Fe}_2\text{Si}$ phase was heterogeneously nucleated on the Fe_2Al_5 phase and grew to an Fe diffusion layer in the Al melt (Figure 7d,e). As the aluminizing temperature increased to 800 and 850 °C, the block-shaped $\text{Al}_8\text{Fe}_2\text{Si}$ phase was preferentially formed. As the temperature increased, the diffusion coefficient also increased, leading to a more active dissolution of the Fe_2Al_5 layer in the Al melt. The diffusion of Al atoms toward the STS420 substrate was dominant at 700 and 750 °C, and the thickness of the reaction layer increased with increasing reaction time. However, at 800 °C and 850 °C, the thickness of Fe_2Al_5 remained relatively constant, depending only on the holding time. During the interaction of STS420 with the molten AC4C melt, an Fe_2Al_5 layer formed and simultaneously dissolved into the molten AC4C. The simultaneous dissolution into the Al melt during the growth of the Fe_2Al_5 phase was confirmed using synchrotron radiation techniques by Zhang et al. [22]. Therefore, the thickness of the Fe_2Al_5 layer is determined by the competition between growth and dissolution. At reaction temperatures of 700 and 750 °C, the formation of the Fe_2Al_5 phase driven by atomic diffusion may be more dominant, and its thickness is believed to increase with reaction time. However, at temperatures above 800 °C, the crystal structure of STS420 (Fe–13Cr) can transform from a body-centered cubic (BCC) to a face-centered cubic (FCC) structure, in which atomic diffusion is relatively challenging [23]. The thickness of the reaction layer developed during hot-dipping or annealing depends on the atomic diffusion rate. Al diffusion is slower in FCC Fe than in BCC Fe by two orders of magnitude [13]. This change in the crystal structure resulted in a

balance between the formation of the Fe_2Al_5 phase and its dissolution in the Al melt, thus maintaining the thickness of the Fe_2Al_5 layer despite the elevated aluminizing temperature.

Figure 8a shows the variations in the cross-section of the STS420 rods in AC4C/STS420 bimetals under various hot-dip aluminizing conditions. The reduction rate R for the STS420 rods was determined using the equation provided [11]:

$$R = A_0B/t \quad (1)$$

where A_0 is the initial area of the STS420 rod cross-section (78.5 mm^2), R is the reduction rate (Figure 8b), and t is the hot-dip aluminizing time. As the reaction temperature increased from $700 \text{ }^\circ\text{C}$ to $850 \text{ }^\circ\text{C}$, the area reduction rate increased from 0.09 to $0.33 \text{ mm}^2 \text{ min}^{-1}$.

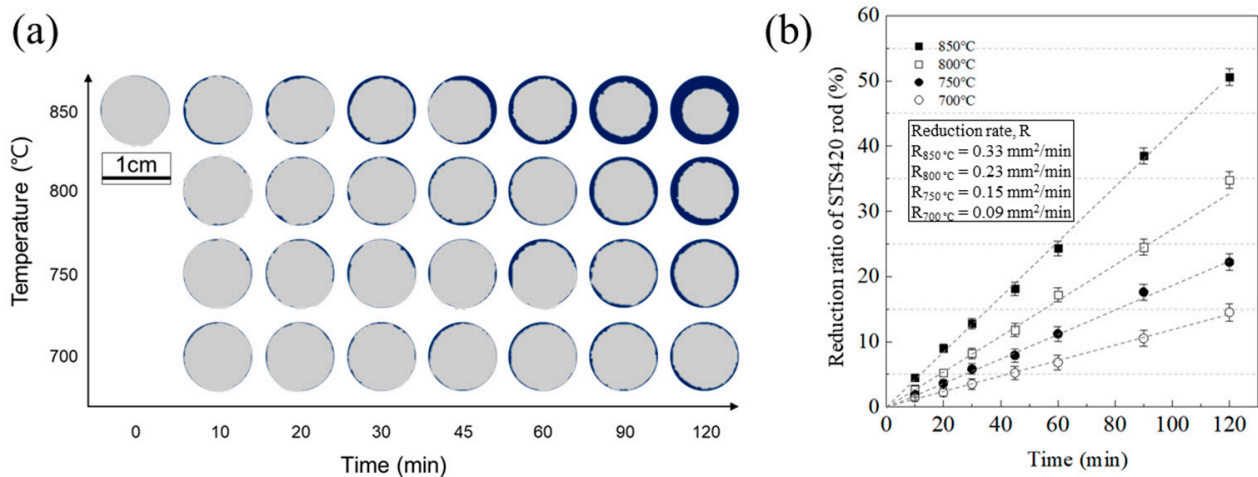


Figure 8. (a) Change in cross-section of STS rods in AC4C/STS420 bimetals with different aluminizing conditions; (b) area reduction ratio of STS420 rod under varying reaction temperatures and holding times.

The cross-sectional area of the STS420 rod decreased proportionately with the increases in reaction temperature and holding time. While approximately 14% of the STS420 rods dissolved during reaction at $700 \text{ }^\circ\text{C}$ for 120 min, approximately 50% of the STS420 rods dissolved when the reaction temperature was increased to $850 \text{ }^\circ\text{C}$. The above results indicate that the high reaction temperature enhances the diffusion of Cr and Fe elements from the STS 420 rod into the molten aluminum alloy. At relatively low reaction temperatures of 700 and $750 \text{ }^\circ\text{C}$, both the aluminizing time and thickness of the reaction layer (Fe_2Al_5 and $\text{Al}_8\text{Fe}_2\text{Si}$) increased simultaneously. This is consistent with previous studies that reported that the IMC thickness increases proportionally with reaction temperature and time [24,25]. However, at relatively high reaction temperatures of 800 and $850 \text{ }^\circ\text{C}$, the Fe_2Al_5 layer formed during the hot-dipping process of the Al–Si/STS bimetal maintained a relatively constant thickness, even upon increasing the holding time (Figure 6b). For short reaction times (10–20 min), the thickness of the Al–Si/STS reaction layer increased with increasing reaction temperature because of the increasing diffusion coefficient [26,27], which in turn was attributed to an increase in the diffusion layer with increasing temperature. Therefore, sufficient heating and holding time are required to ensure sufficient atomic diffusion between the interacting liquid and solid components [21]. However, during the formation of Fe_2Al_5 layers in the course of the hot-dipping process, these IMCs lost their atomic components to the Al melt and eventually dissolved. This decomposition of the Fe_2Al_5 phases occurred more vigorously at the relatively higher temperatures of 800 and $850 \text{ }^\circ\text{C}$, which can be attributed to the greater thickness reduction in the STS rods at higher temperatures owing to greater diffusion. In addition, at the same time, the solubility of the Fe_2Al_5 layer in the molten Al alloy increased, creating a high-Fe diffusion region near the STS420 substrate during the aluminizing process. As a result, the thickness of the IMC

layer was maintained by balancing its formation in the high-Fe diffusion region (increasing thickness) near the STS420 rod and dissolution into the Al melt (decreasing thickness). Therefore, even when the reaction time was prolonged, the thickness of the Fe_2Al_5 phase formed during the immersion process did not change significantly, whereas the $\text{Al}_8\text{Fe}_2\text{Si}$ phase formed during the solidification process showed coarser growth owing to an increase in the Fe content diffused near the STS420 substrate. Previous studies [10,28] have also reported that a coarse blocky Al–Fe–Si phase with a high concentration of atomic diffusion regions forms in Al–Si alloy melts during the hot-dip aluminizing process.

Figure 9 displays the hardness values of the AC4C/STS420 bimetals interface formed under different aluminizing conditions (700 and 850 °C for 10 and 120 min). The hardness of the IMCs exhibits much higher values than those of the STS420 and AC4C matrix. The high hardness of the aluminized layer indicates the formation of hard intermetallic phases. The STS, Fe_2Al_5 , $\text{Al}_8\text{Fe}_2\text{Si}$, and Al phases exhibited hardness values of approximately 300, 1260, 1130, and 75 HV, respectively. Therefore, it is apparent that the significantly higher hardness of the AC4C/STS420 interface compared with the metallic materials STS420 and AC4C was due to the formation of Fe_2Al_5 and $\text{Al}_8\text{Fe}_2\text{Si}$ phases. Slightly differing from these results, the Fe_2Al_5 phase of Al/Fe bimetals typically exhibits a microhardness value of approximately 1000 HV [7]. Troysi et al. [29] have reported that the Fe_2Al_5 phase of aluminized 1020 steel (with a Cr composition of approximately 0.03 wt.%) exhibits a hardness value of 1070 HV. However, in this study, the $\text{Fe}_2\text{Al}_5(\text{Cr})$ layer in Al–Si–Mg/STS420 bimetals exhibits a hardness of approximately 1260 HV, which is about 20% higher than that of the Fe_2Al_5 layer in Al/Fe bimetals. This hardness increase is probably due to the strengthening effect of Cr in $\text{Fe}_2\text{Al}_5(\text{Cr})$ and Cr-rich precipitates. Similarly, the hardness values of the $\text{Fe}_2\text{Al}_5(\text{Cr})$ phase of Al/STS bimetals containing Cr-rich precipitates were reported to range approximately from 1143 to 1250 HV [30]. A rapid increase in the hardness at the interface between the metallic materials and the IMCs leads to stress singularities [31,32]. At the interface between the STS420 matrix and top Al coat, a gradual change in hardness was observed; as the thickness of the reaction layer increased, the hardness gradient also increased (Figure 9). Therefore, the hardness gradient corresponds to the change in the thickness of the reaction layer depending on the aluminizing temperature and holding time, as shown in Figure 6. Previous studies have also reported that the thickness and hardness gradient of the Al/Fe reaction layer increase with increasing temperature [33,34]. The reaction layer was thicker when reacted at 700 °C for 90 min and 750 °C for 60 min than when reacted at higher temperatures (800–850 °C). In addition, at 800–850 °C, block-shaped IMCs formed, which are prone to stress concentration [35], and the shape of the reaction layer changed from linear to wavy. In our study, the hardness profile of the aluminized Fe_2Al_5 reaction layer gradually increased with increasing aluminizing time at 700 °C (Figure 9a) but remained relatively uniform at 850 °C (Figure 9b). Thinner reaction layers deform more easily than thicker reaction layers, and flatter reaction layers impart Al/Fe bimetals with better hardness properties by relieving stress concentrations during the aluminizing process [2,10,36]. Therefore, AC4C/STS420 bimetals aluminized for short periods at low temperatures (specifically, 700 °C for 10–20 min in this study) are expected to exhibit superior hardness properties to those aluminized at higher temperatures.

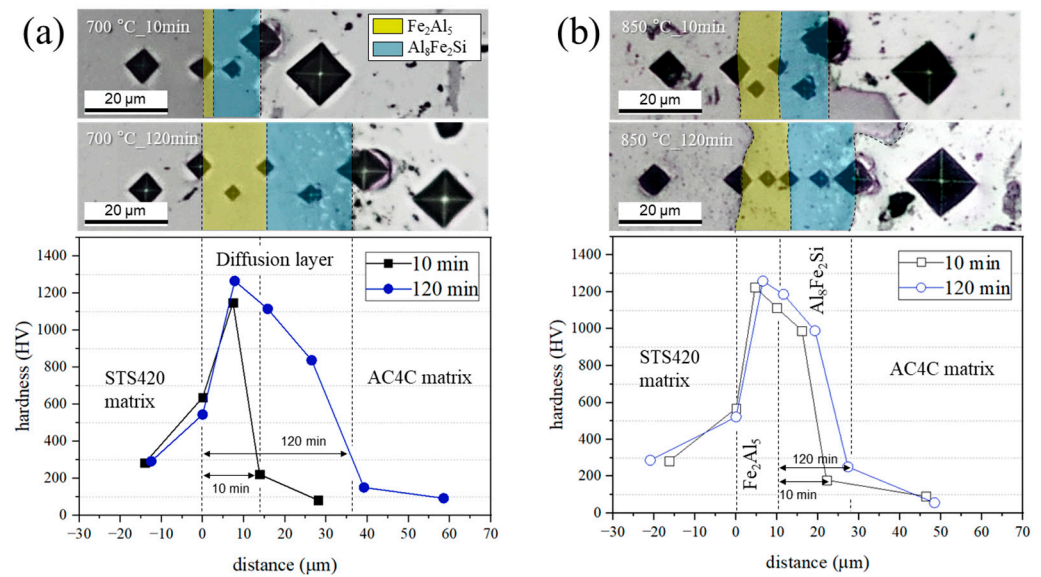


Figure 9. Vickers hardness values of AC4C/STS420 bimetals fabricated at different aluminizing temperatures for 10 and 120 min: (a) 700 °C and (b) 850 °C.

4. Conclusions

In this study, we investigated the interfacial region of aluminized STS420 rods in Al-Si-Mg alloy melt, including the formation mechanism of IMC phase and the effects of the aluminizing parameters on the IMC morphologies and hardness. The key findings of our investigation are as follows.

The proposed formation mechanism of AC4C/STS420 IMC during the aluminizing process is as follows: Fe₂Al₅ initially appears during the aluminizing process in the AC4C melt, and Al₈Fe₂Si is grown after the aluminized STS rods are lifted out of the AC4C melt.

As the reaction temperature increased, the uniform flat Fe₂Al₅ and Al₈Fe₂Si layers changed to exhibit wavy and blocked morphologies, respectively. At low reaction temperatures (700 and 750 °C), the thickness of the reaction layer gradually increased with increasing reaction time, whereas it remained relatively constant at high temperatures (800 and 850 °C).

The thickness and morphology of the IMC layer influence the hardness profile of the AC4C/STS420 bimetals interface. The hardness value of the IMCs layer was much higher than that of the metal matrix (STS420 and AC4C), and as the thickness of the reaction layer increased, the hardness gradient of the layer also increased. Therefore, this study suggested that the aluminizing conditions to form a fine and uniform reaction layer should be 10 to 20 min at 700 °C.

Author Contributions: Conceptualization, Y.-S.L.; methodology, H.-Y.L.; investigation, H.-Y.L. and S.H.K.; resources, S.-H.K.; data curation, B.-J.K.; writing—original draft preparation, B.-J.K.; writing—review and editing, B.-J.K. and Y.-S.L.; visualization, B.-J.K.; supervision, S.-H.K.; project administration, Y.-S.L.; funding acquisition, Y.-S.L., J.-H.C. and S.-H.K. All authors have read and agreed to the published version of the manuscript.

Funding: This research was funded by the Fundamental Research Program of the Korea Institute of Materials Science, grant number PNK9840, and National Research Foundation of Korea (NRF) grants funded by the Korean government (MSIP), grant number NRF-2021M3H4A1A04091999.

Data Availability Statement: The raw data supporting the conclusions of this article will be made available by the authors on request.

Conflicts of Interest: The authors declare no conflicts of interest.

References

1. Wang, C.; Wang, Z.; Xu, H.; Zhang, G. Microstructure and Age Hardening Behavior of Al/Fe Bimetal Prepared by One-Step Compound Casting. *J. Alloys Compd.* **2022**, *905*, 164170. [[CrossRef](#)]
2. Chen, Q.; Chang, X.; Qi, L.; Zheng, J.; Xie, C.; Chen, G. Interface Heterogeneity of Aluminum-Steel Bimetal Parts Manufactured via Thixotropic-Core Compound Forging. *J. Mater. Process. Technol.* **2022**, *306*, 117648. [[CrossRef](#)]
3. Chang, X.; Chen, G.; Wang, B.; Chen, Q.; Zhang, H. Thixotropic-Core Compound Forging for Aluminum-Steel Bimetal Gears. *J. Mater. Process. Technol.* **2022**, *299*, 117371. [[CrossRef](#)]
4. Jiang, W. Effects of Hot-Dip Galvanizing and Aluminizing on Interfacial Microstructures and Mechanical Properties of Aluminum/Iron Bimetallic Composites. *J. Alloys Compd.* **2016**, *688*, 742–751. [[CrossRef](#)]
5. Mao, F.; Zhang, P.; Wei, S.; Chen, C.; Zhang, G.; Xiong, M.; Wang, T.; Guo, J.; Wang, C. Interface Microstructure and Mechanical Properties of Al/Steel Bimetallic Composites Fabricated by Liquid-Solid Casting with Rare Earth Eu Additions. *Materials* **2022**, *15*, 6507. [[CrossRef](#)] [[PubMed](#)]
6. Kepa, T.; Pedraza, F.; Rouillard, F. Intermetallic Formation of Al-Fe and Al-Ni Phases by Ultrafast Slurry Aluminization (Flash Aluminizing). *Surf. Coat. Technol.* **2020**, *397*, 126011. [[CrossRef](#)]
7. Dey, P.P.; Sahu, S.; Banerjee, P.S.; Ghosh, M. A Review on Metallurgical Features of Hot-Dip Aluminized Steel. *Eng. Res. Express* **2023**, *5*, 012002. [[CrossRef](#)]
8. Liberski, P.; Gierek, A.; Kania, H.; Podolski, P.; Tatarek, A. Formation of Coatings from a Liquid Phase on the Surface of Iron-Base Alloys. *Arch. Foundry Eng.* **2008**, *8*, 93.
9. Khalid, M.Z.; Friis, J.; Ninive, P.H.; Marthinsen, K.; Ringdalen, I.G.; Strandlie, A. Modified Embedded Atom Method Potential for Fe-Al Intermetallics Mechanical Strength: A Comparative Analysis of Atomistic Simulations. *Phys. B Condens. Matter* **2021**, *618*, 413157. [[CrossRef](#)]
10. Cheng, W.-J.; Wang, C.-J. Effect of Silicon on the Formation of Intermetallic Phases in Aluminide Coating on Mild Steel. *Intermetallics* **2011**, *19*, 1455–1460. [[CrossRef](#)]
11. Kim, B.-J.; Cheon, H.-S.; Lee, Y.-H.; Kim, W.-K.; Lee, Y.-S.; Kim, S.-H. Effect of Reaction Temperature and Holding Time on the Interfacial Microstructure of Al-Si-Mg/Cu Bimetals Manufactured by Hot-Dip Aluminizing. *Mater. Chem. Phys.* **2024**, *313*, 128758. [[CrossRef](#)]
12. Wang, H.; Sun, S.; Li, X.; Wang, J.; Su, X. Effect of Silicon on Interfacial Reaction and Morphology of Hot-Dip Aluminizing. *J. Mater. Res. Technol.* **2022**, *20*, 3723–3734. [[CrossRef](#)]
13. Prasanthi, T.N.; Sudha, C.; Reddy, P.S. Hot Dip Aluminization of 304L SS and P91 Ferritic-Martensitic Steel—Comparison of Interface Morphology and Growth Kinetics of Reaction Zones. *Surf. Coat. Technol.* **2022**, *440*, 128465. [[CrossRef](#)]
14. Chang, Y.-Y.; Tsaur, C.-C.; Rock, J.C. Microstructure Studies of an Aluminide Coating on 9Cr-1Mo Steel during High Temperature Oxidation. *Surf. Coat. Technol.* **2006**, *200*, 6588–6593. [[CrossRef](#)]
15. Divandari, M.; Vahid Golpayegani, A.R. Study of Al/Cu Rich Phases Formed in A356 Alloy by Inserting Cu Wire in Pattern in LFC Process. *Mater. Des.* **2009**, *30*, 3279–3285. [[CrossRef](#)]
16. Liu, B.; Yang, Q.; Wang, Y. Intereaction and Intermetallic Phase Formation between Aluminum and Stainless Steel. *Results Phys.* **2019**, *12*, 514–524. [[CrossRef](#)]
17. Yang, Y.; Zhong, S.-Y.; Chen, Z.; Wang, M.; Ma, N.; Wang, H. Effect of Cr Content and Heat-Treatment on the High Temperature Strength of Eutectic Al-Si Alloys. *J. Alloys Compd.* **2015**, *647*, 63–69. [[CrossRef](#)]
18. Shabestari, S. The Effect of Iron and Manganese on the Formation of Intermetallic Compounds in Aluminum-Silicon Alloys. *Mater. Sci. Eng. A* **2004**, *383*, 289–298. [[CrossRef](#)]
19. Sha, M.; Wu, S.; Wang, X.; Wan, L. Effects of Co Addition on Fe-Bearing Intermetallic Compounds and Mechanical Properties of AlSi20Cu2Ni1Fe0.7–1 Alloys. *J. Alloys Compd.* **2013**, *551*, 468–474. [[CrossRef](#)]
20. Hosseiniifar, M.; Malakhov, D.V. The Sequence of Intermetallics Formation during the Solidification of an Al-Mg-Si Alloy Containing La. *Met. Mater. Trans A* **2011**, *42*, 825–833. [[CrossRef](#)]
21. Palm, M. The Al-Cr-Fe System—Phases and Phase Equilibria in the Al-Rich Corner. *J. Alloys Compd.* **1997**, *252*, 192–200. [[CrossRef](#)]
22. Zhang, N.; Hu, Q.; Yang, F.; Lu, W.; Ding, Z.; Cao, S.; Yu, L.; Ge, X.; Li, J. Effect of Si on the Growth Behavior of the Fe₂Al₅ Phase at Al-xSi(Liquid)/Fe(Solid) Interface During Holding by In-Situ Synchrotron Radiography. *Met. Mater. Trans A* **2020**, *51*, 2711–2718. [[CrossRef](#)]
23. Xiong, W.; Selleby, M.; Chen, Q.; Odqvist, J.; Du, Y. Phase Equilibria and Thermodynamic Properties in the Fe-Cr System. *Crit. Rev. Solid State Mater. Sci.* **2010**, *35*, 125–152. [[CrossRef](#)]
24. Bakke, A.O.; Arnberg, L.; Løland, J.-O.; Jørgensen, S.; Kvinge, J.; Li, Y. Formation and Evolution of the Interfacial Structure in Al/Steel Compound Castings during Solidification and Heat Treatment. *J. Alloys Compd.* **2020**, *849*, 156685. [[CrossRef](#)]
25. Dey, P.P.; Modak, P.; Ghosh, A.; Chakrabarti, D.; Banerjee, P.S.; Ghosh, M. Investigation of Phase Evolution of Al-Si-Mg Coating on Hot Dipped Interstitial-Free Steel. *Results Mater.* **2020**, *6*, 100078. [[CrossRef](#)]
26. Liu, T.; Wang, Q.; Sui, Y.; Wang, Q.; Ding, W. An Investigation into Interface Formation and Mechanical Properties of Aluminum-Copper Bimetal by Squeeze Casting. *Mater. Des.* **2016**, *89*, 1137–1146. [[CrossRef](#)]
27. Mao, A.; Zhang, J.; Yao, S.; Wang, A.; Wang, W.; Li, Y.; Qiao, C.; Xie, J.; Jia, Y. The Diffusion Behaviors at the Cu-Al Solid-Liquid Interface: A Molecular Dynamics Study. *Results Phys.* **2020**, *16*, 102998. [[CrossRef](#)]

28. Zarei, F.; Nuranian, H.; Shirvani, K. Effect of Si Addition on the Microstructure and Oxidation Behaviour of Formed Aluminide Coating on HH309 Steel by Cast-Aluminizing. *Surf. Coat. Technol.* **2020**, *394*, 125901. [[CrossRef](#)]
29. Troysi, F.D.; Brito, P.P. Development and Characterization of an Iron Aluminide Coating on Mild Steel Substrate Obtained by Friction Surfacing and Heat Treatment. *Int. J. Adv. Manuf. Technol.* **2020**, *111*, 2569–2576. [[CrossRef](#)]
30. Kishore, K.; Chhangani, S.; Prasad, M.J.N.V.; Bhanumurthy, K. Microstructure Evolution and Hardness of Hot Dip Aluminized Coating on Pure Iron and EUROFER 97 Steel: Effect of Substrate Chemistry and Heat Treatment. *Surf. Coat. Technol.* **2021**, *409*, 126783. [[CrossRef](#)]
31. Chi, S.-H.; Chung, Y.-L. Mechanical Behavior of Functionally Graded Material Plates under Transverse Load—Part I: Analysis. *Int. J. Solids Struct.* **2006**, *43*, 3657–3674. [[CrossRef](#)]
32. Bhavar, V.; Kattire, P.; Thakare, S.; patil, S.; Singh, R. A Review on Functionally Gradient Materials (FGMs) and Their Applications. *IOP Conf. Ser.: Mater. Sci. Eng.* **2017**, *229*, 012021. [[CrossRef](#)]
33. Zhang, D.; Zhang, G.; Yu, H.; Lv, W.; Wen, K.; Xu, H. Controlling Interfacial Composition and Improvement in Bonding Strength of Compound Casted Al/Steel Bimetal via Cr Interlayer. *J. Mater. Res. Technol.* **2023**, *23*, 4385–4395. [[CrossRef](#)]
34. Lou, B.-S.; Chen, Y.-Y.; Wu, Z.-Y.; Kuo, Y.-C.; Duh, J.-G.; Lee, J.-W. (Fe,Mn)₃AlC_x κ-Carbide Formation and Characterization in Pack Aluminization of Fe–29Mn–9Al–0.9C Lightweight Steel. *J. Mater. Res. Technol.* **2022**, *20*, 1524–1532. [[CrossRef](#)]
35. Kim, B.J.; Dahle, A.K.; Park, Y.H.; Lee, Y.C. The Effect of Sr Additions on Al–Cu–Si Ternary Eutectic Alloys for a High-Ductility Bimodal Microstructure. *Mater. Sci. Eng. A* **2022**, *833*, 142547. [[CrossRef](#)]
36. Guo, Z.; Liu, M.; Bian, X.; Liu, M.; Li, J. An Al–7Si Alloy/Cast Iron Bimetallic Composite with Super-High Shear Strength. *J. Mater. Res. Technol.* **2019**, *8*, 3126–3136. [[CrossRef](#)]

Disclaimer/Publisher’s Note: The statements, opinions and data contained in all publications are solely those of the individual author(s) and contributor(s) and not of MDPI and/or the editor(s). MDPI and/or the editor(s) disclaim responsibility for any injury to people or property resulting from any ideas, methods, instructions or products referred to in the content.